

Supporting Information

3- and 4-(α -Diazobenzyl)pyridine-*N*-oxide as Photoresponsive Magnetic Couplers for 2p - 4f Heterospin Systems: Formation of Carbene-Tb^{III} and Carbene-Dy^{III} Single-molecule Magnets.

Kensuke Murashima, Satoru Karasawa*, Kenji Yoza, Yuji Inagaki,
and Noboru Koga*.

*Corresponding authors: Tel +81-92-642-6590. Fax +81-92-642-6590

E-mail: koga@fc.phar.kyushu-u.ac.jp

karasawa@fc.phar.kyushu-u.ac.jp

Contents.

S-1. Figure S1. Solid-state absorption spectra of **1d**, **2d**, **2'd**, and **3d**.

S-2. Figure S2. ORTEP drawings of **2d**, **2'd**, and **3d**.

S-3. Coordination geometries

Table S1. Bond lengths and bond angles for **1d**, **2d**, **2'd**, and **3d**.

Table S2. Shape measurement analyses for **1d**, **2d**, **2'd**, and **3d**.

S-4. Figure S3. ORTEP drawings and crystal packings of **2'd**.

S-5. Figure S4. ESR spectra (9.0 GHz) after irradiation of **4-D1pyO** and **3-D1pyO** in MTHF.

S-6. Figure S5. PXRD patterns of **1d**, **2d**, and **3d**, and the simulation obtained from SXRD of **1d**.

S-7. Figure S6. Plots of $\chi_{\text{mol}}T$ vs. Irradiation time for **1d**, **2d**, **2'd**, and **3d**.

S-8. Figure S7. $\chi_{\text{mol}}T$ vs. T plots before irradiation of **1d**, **2d**, and **3d**. (sample A) with the best fitting result for **1d**.

S-9. Equation S1 and estimation of exchange coupling constants for **1d** and **1c**.

Scheme S1. A rhombic four-spin model for **1c**.

Figure S8. $\chi_{\text{mol}}T$ vs. T plots before and after irradiation of **2d** with the best fit results.

S-10. Figure S9. $\chi_{\text{mol}}T$ vs. T plots before and after irradiation of **2'd**.

S-11. Figure S10. M_{mol} vs. H/T plots before and after irradiation of **1d**, **2d**, **2'd**, and **3d**.

S-12. Figure S11. Plots of $\chi'_{\text{mol}}T$ vs. T and χ''_{mol} vs. T in the absence and presence of dc field before irradiation of **2d**.

S-13. Table S3. Parameters for **2c** calculated by an extended Debye model.

S-14. Figure S12. Plots of χ'_{mol} vs. *frequency* and χ''_{mol} vs. *frequency*, and Cole – Cole of **2c**.

S-15. Analysis of Cole – Cole plots for **2c** with a multiple relaxation process (equation S2).

Table S4. Parameters of **2c** obtained from the fitting with the equation S2 for a multiple relaxation process.

Figure S13. Arrhenius plots for two species for **2c**.

S-16. Figure S14. Plots of $\chi'_{\text{mol}}T$ vs. T and χ''_{mol} vs. T of **2'c**.

S-17. Table S5. The parameters for **3c** calculated by an extended Debye model.

S-18. Figure S15 Plots of χ'_{mol} vs. *frequency*, χ''_{mol} vs. *frequency*, and Cole – Cole of **3d** and **3c**.

S-19. References.

S-1.

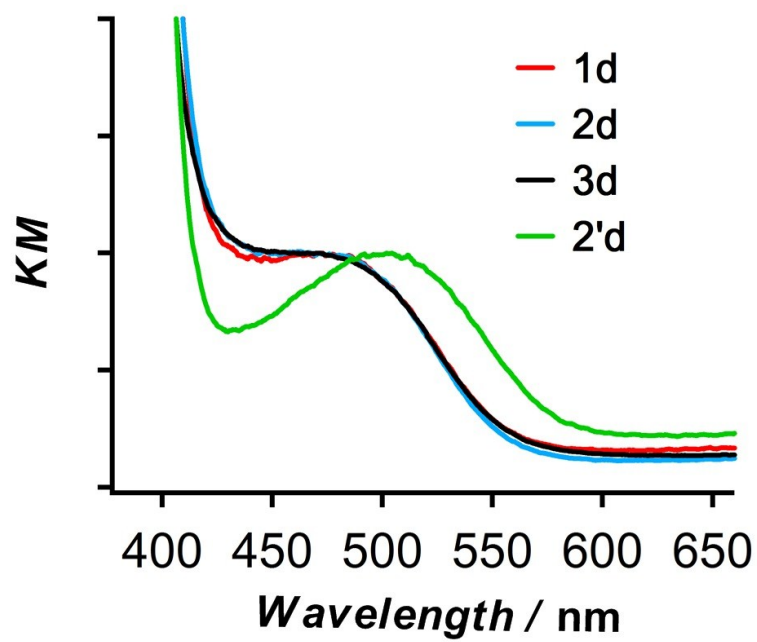
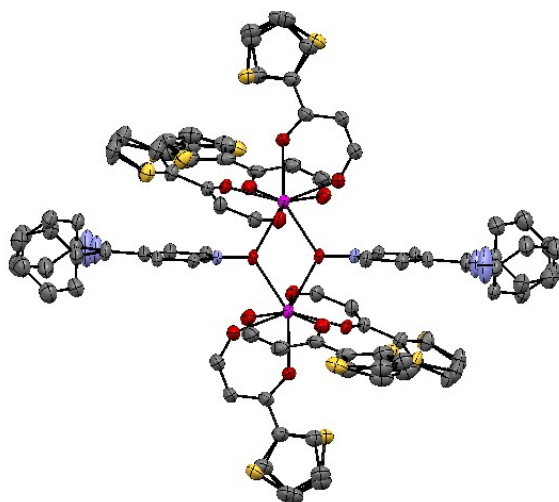


Figure S1. Solid-state absorption spectra of 1d, 2d, 2'd, and 3d.

S-2.

(a)



(b)

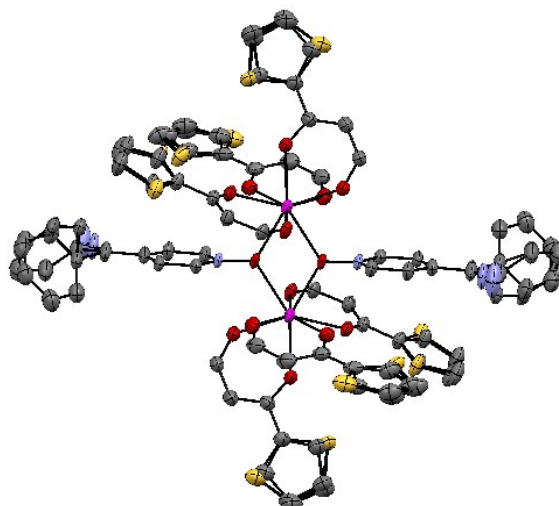


Figure S2. ORTEP drawing (50% probability) of molecular structures of **2d** (a) and **3d** (b).

S-3. Coordination geometries of **1d**, **2d**, **2'd**, and **3d**.

The angles of least square planes (P1 for O(2)O(3)O(4)O(5) and P2 for O(1)O(1)*O(6)O(7)) defined by the four oxygen atoms, were 4.71(2) ° and 7.65(2) °, respectively, and the dihedral angle between P1 and P2 was 4.95 (11) °, indicating that the planes of P1 and P2 were almost ideal (0 °) and the planes were stacked in parallel. Furthermore, the average angle between the eight triangle planes defined by the one or two oxygen atoms in P1 and P2 was 52 (5) °. Even though ESD of the angle was somehow large, the average angle was close to that for an ideal square antiprism structure with the D_{4d} symmetry. Angles for **2d**, **2'd**, and **3d** were similar to those for **1d**, which are listed in Table S1. To confirm the precise geometry of the polyhedrons of the complexes, calculation of the degree of deviation for the Ln^{III} coordination polyhedron from the ideal eight-vertex Ln^{III} structure was conducted using the continuous shape measure theory and SHAPE software.²³ The result for **1d** indicated low values for square antiprism (0.993, D_{4d}), triangular dodecahedron (1.021, D_{2d}), and biaugmented trigonal prism (1.871, C_{2v}) (Table S2). Therefore, the coordination geometry might be a distorted square antiprism structure.

Table S1. Bond lengths, bond angles, square plane angles, dihedral angles, and intermolecular Ln^{III}-Ln^{III} distances for **1d**, **2d**, **2'd**, and **3d**.

	1d	2d	2'd	3d
Bond lengths / Å				
Ln(1)-O(1)	2.4112(2)	2.40616(9)	2.3894(6)	2.3853(1)
Ln(1)-O(1)*	2.421(3)	2.4078(1)	2.455(5)	2.4013(1)
Ln(1)-O(2)	2.318(3)	2.3049(1)	2.321(5)	2.2899(1)
Ln(1)-O(3)	2.376(3)	2.3717(1)	2.354(5)	2.3605(2)
Ln(1)-O(4)	2.378(3)	2.3600(1)	2.335(5)	2.3478(1)
Ln(1)-O(5)	2.382(3)	2.3720(1)	2.364(5)	2.3507(2)
Ln(1)-O(6)	2.350(4)	2.32951(9)	2.330(5)	2.3155(1)
Ln(1)-O(7)	2.397(3)	2.3843(1)	2.335(5)	2.3778(1)
N(1)-O(1)	1.3555(1)	1.34693(7)	1.365(8)	1.3598(1)
Ln(1)-Ln(1)*	4.1294(3)	4.1112(2)	4.1289(7)	4.0922(3)
O _{pyO} -O _{pyO} *	2.510(3)	2.5044(1)	2.535(5)	2.4830(2)
Bond angle / °				
O _{pyO} -Ln- O _{pyO}	62.58(7)	62.697(3)	63.09(11)	62.494(5)
Ln- O _{pyO} -Ln	117.42(12)	117.303(3)	116.9(2)	117.506(5)
Square plane angles / °				
P1: O(2)O(3)O(4)O(5)	4.71(2),	4.9758(4),	2.65(2),	4.9896 (4),

P2: O(1)O(1)*O(6)O(7)	7.65(2)	7.8749(4)	5.83 (2)	7.9041(4)
Dihedral angles / °				
P1-P2	4.95(11)	3.918(3)	3.66(15)	3.848(3)
Triangle**	52(5)	51(6)	51(3)	52(6)
C(1)C(3)C(5)N(1)- C(3)C(6)N(2)N(3)	5.0(5)	5.557(8)	16.4(6)	4.450(7)
LnO _{py} O Ln*O _{py} O* C(1)N(1)C(3)C(5)	91.0(1)	90.367(3)	90.4 (2)	90.598(4)
Intermolecular Ln ^{III} -Ln ^{III} distances (Å)				
Ln(1)-Ln(1)***	12.0524(7)	12.7290(5)	9.733	12.07

* the atoms corresponding to symmetry of inversion center (-x, -y, -z).

** the average dihedral angles between the triangles in distorted antiprism polyhedron

*** the atoms corresponding to symmetry of 2-fold screw axis (1/2 + x, 1/2 - y, 1/2 + z) and (-1/2-x, -1/2+y, -1/2-z).

Table S2. Shape measurement analyses for **1d**, **2d**, **2'd**, and **3d**.

[ML8]	OP-8	HPY-8	HBPY-8	CU-8	SAPR-8	TDD-8	JGBF-8	JETBPY-8	JBTPR-8	BTPR-8	JSD-8	TT-8
1d	30.637	23.195	16.725	9.707	0.993	1.021	14.906	28.942	2.503	1.871	3.587	10.388
2d	30.308	23.257	16.643	9.612	0.931	1.050	15.016	28.798	2.479	1.875	3.600	10.279
3d	30.480	23.356	16.480	9.552	0.977	0.991	15.026	28.726	2.447	1.874	3.531	10.232
2'd	30.367	22.745	16.311	10.589	0.691	1.708	15.096	28.335	2.445	1.814	4.084	11.378

OP-8	1, D8h	Octagon
HPY-8	2, C7v	Heptagonal pyramid
HBPY-8	3, D6h	Hexagonal bipyramid
CU-8	4, Oh	Cube
SAPR-8	5, D4d	Square antiprism
TDD-8	6, D2d	Triangular dodecahedron
JGBF-8	7, D2d	Johnson gyrobifastigium J26
JETBPY-8	8, D3h	Johnson elongated triangular bipyramid J14
JBTPR-8	9, C2v	Biaugmented trigonal prism J50
BTPR-8	10, C2v	Biaugmented trigonal prism
JSD-8	11, D2d	Snub diphenoid J84
TT-8	12, Td	Triakis tetrahedron

S-4.

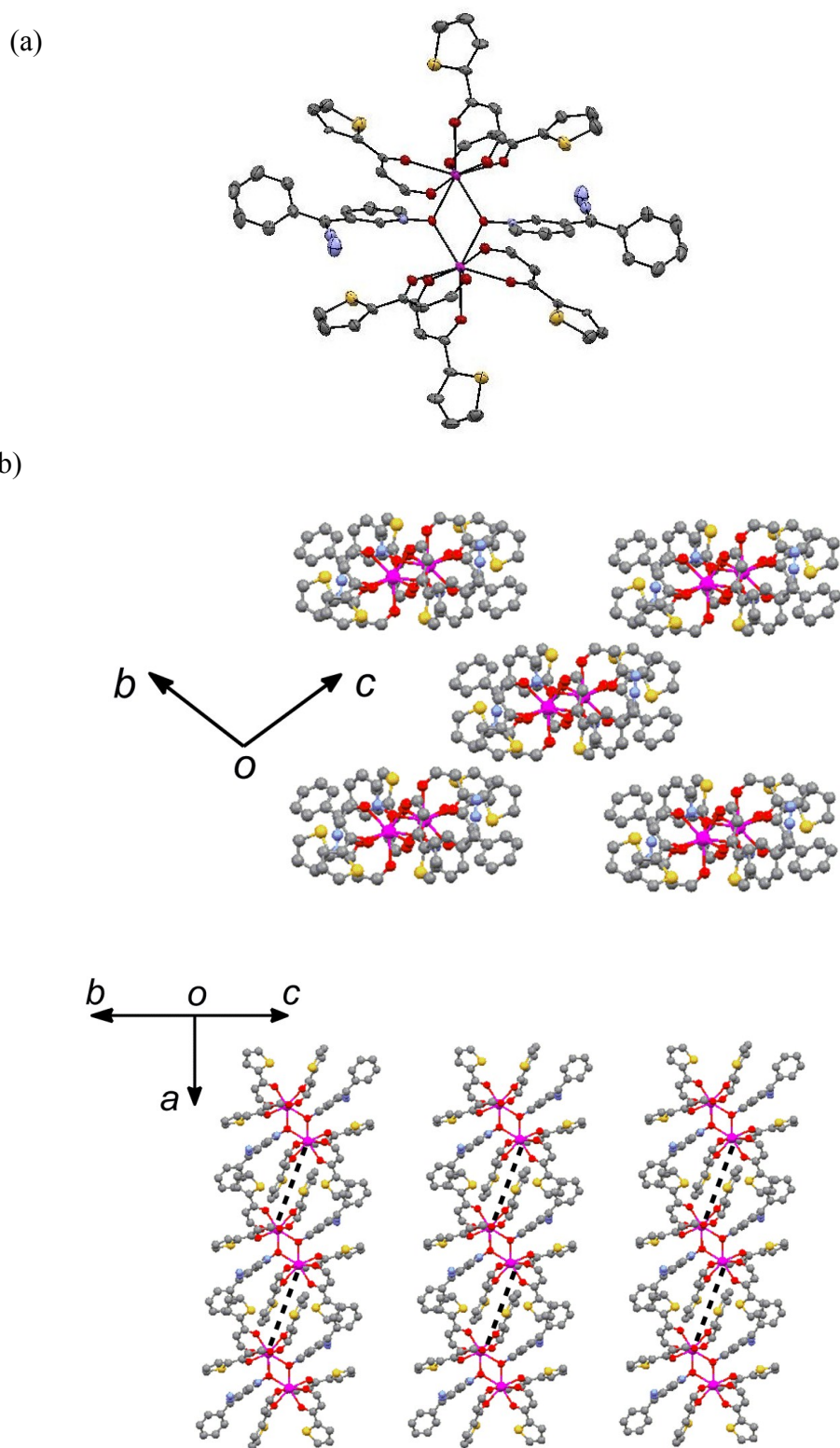


Figure S3. ORTEP drawing (50 % probability) of molecular structure (a) and crystal packings (b) of **2'd**. The dotted lines in (b) indicate the shortest intermolecular distances between the Tb^{III} ions by 12.73(1) Å.

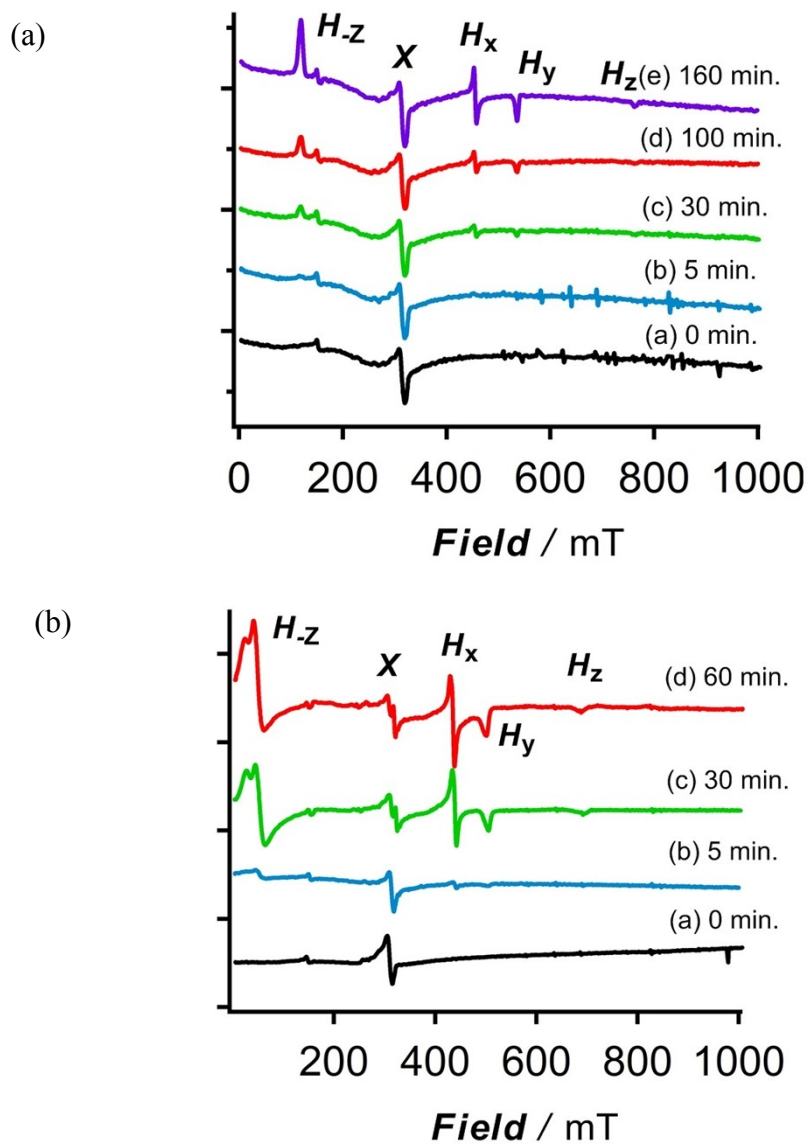


Figure S4. Alteration of ESR spectra (9.0 GHz) by irradiation of **3-D1pyO** (a) and **4-D1pyO** (b). Xs indicate impurity of the sample tube.

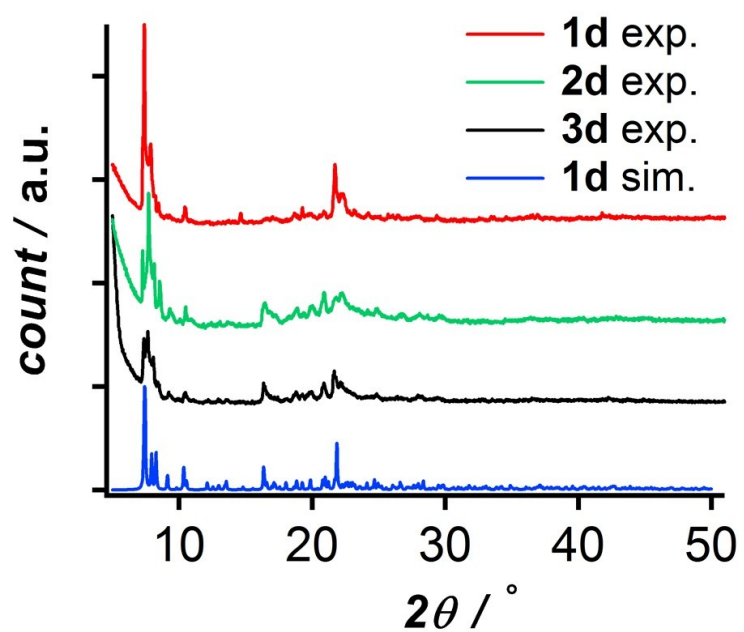


Figure S5. PXRD patterns for the sample B of **1d** (red), **2d** (green), and **3d** (black) together with the simulation pattern obtained from the SXRD data of **1d** (blue).

S-7.

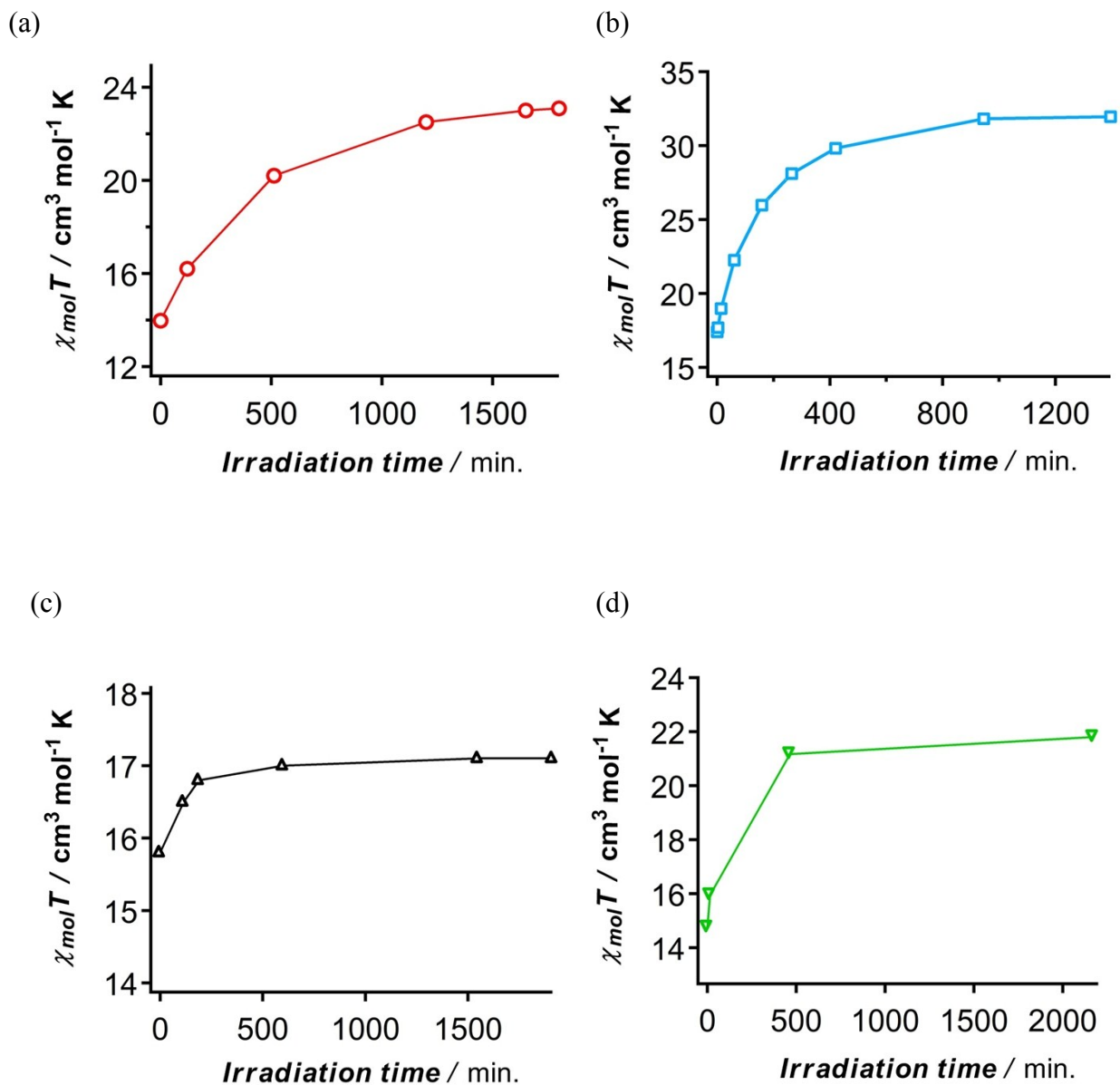


Figure S6. Plots of $\chi_{mol}T$ vs. Irradiation time for **1d** (a), **2d** (b), **2'd** (c), and **3d** (d).

S-8.

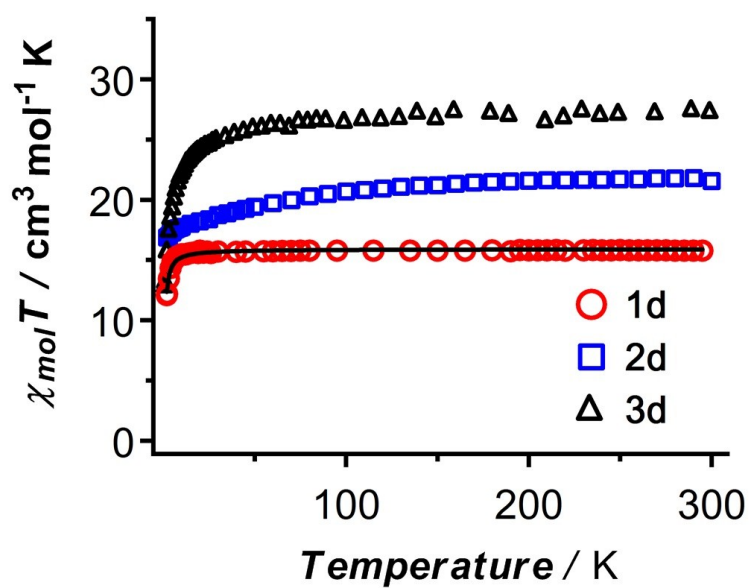


Figure S7. $\chi_{mol}T$ vs. T plots before irradiation of **1d** – **3d**. Black solid line shows best fit result of **1d** according to eq. S1(S-9).

S-9.

Estimation of the exchange coupling constant, $J_{\text{Gd-Gd}}$ in **1d**.

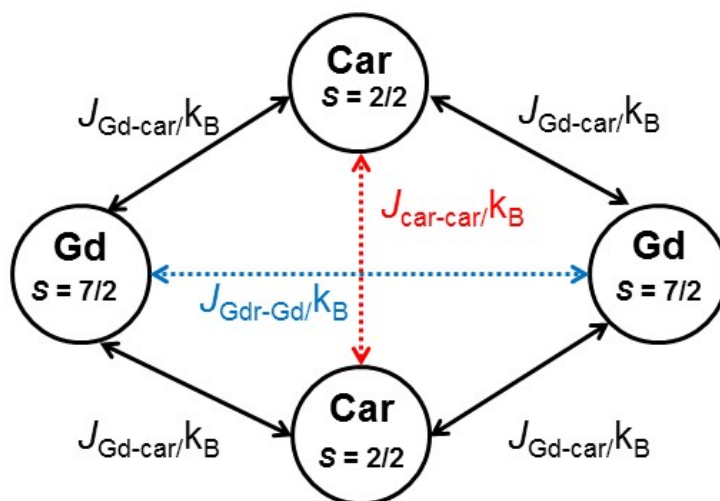
$$H = -J_{\text{Gd-Gd}} (S_{\text{Gd1}} S_{\text{Gd2}})$$

$$\chi_{\text{mol}} T = \frac{2Ng^2\mu_{\text{B}}^2}{k} \frac{140+91e^{7x}+55e^{13x}+30e^{18x}+14e^{22x}+5e^{25x}+e^{27x}}{15+13e^{7x}+11e^{13x}+9e^{18x}+7e^{22x}+5e^{25x}+3e^{27x}+e^{28x}}, \quad x = -J/kT \quad \text{eq. S1}$$

The exchange coupling constant between the Gd ions ($J_{\text{Gd-Gd}}$) within the dinuclear complex was calculated by using eq.S1 derived from the isotropic spin Hamiltonian, where S_{Gd} represents the quantum spin number of Gd^{III} ion ($S = 7/2$). The best fitting result gave $g = 2.01$, and $J_{\text{Gd-Gd}}/k_{\text{B}} = -0.08$ K. The best fit result is shown in Figure S7.

Estimation of the exchange coupling constants, $J_{\text{car-car}}$ and $J_{\text{Gd-car}}$, in **1c**.

To understand the ferromagnetic interaction, the thermal profile in the range of 2 – 30 K was analysed by a FIT-MART program.¹⁾ The spin system for **1c** was considered as a rhombic four-spin model consisting of two carbene centers and two Gd^{III} ions. A rhombic four-spin model had the two through-space interactions of Gd^{III} – Gd^{III} and the carbene – carbene *via* the O - O of *N*-oxides, and the four through-bond interactions of the carbene – Gd^{III} *via* the oxygen atoms of pyridine-*N*-oxide (Scheme S1). Its spin Hamiltonian was expressed as $H = -J_{\text{Gd-Gd}} (S_{\text{Gd1}} S_{\text{Gd2}}) - J_{\text{car-car}} (S_{\text{car1}} S_{\text{car2}}) - J_{\text{Gd-car}} (S_{\text{Gd1}} S_{\text{car1}} + S_{\text{Gd1}} S_{\text{car2}} + S_{\text{Gd2}} S_{\text{car1}} + S_{\text{Gd2}} S_{\text{car2}})$, in which $J_{\text{car-car}}$, $J_{\text{Gd-Gd}}$, and $J_{\text{Gd-car}}$ were the exchange coupling constants between the carbenes with through O-O space, between the Gd^{III} ions through the space, and between the carbene and the Gd^{III} ion through the bonds, respectively. To reduce the number of parameters, the $J_{\text{Gd-Gd}}/k_{\text{B}}$ value was fixed by -0.08 K, which was obtained by using the data before irradiation. The calculation gave $J_{\text{car-car}}/k_{\text{B}} = -8.9$ K and $J_{\text{Gd-car}}/k_{\text{B}} = 2.4$ K, respectively, indicating that the competing magnetic interaction between the through-bond ferromagnetic interactions and the through-space antiferromagnetic interactions took place. The obtained result is shown in Figure S8.



Scheme S1. A rhombic four-spin model consisting of two carbene centers and two Gd^{III} ions. The magnetic interactions of through bonds between carbene and Gd^{III} ion, and the through spaces between two carbenes *via* the oxygen atoms and two Gd^{III} ion represent $J_{\text{Gd-car}}/k_B$, $J_{\text{car-car}}/k_B$, and $J_{\text{Gd-Gd}}/k_B$, respectively.

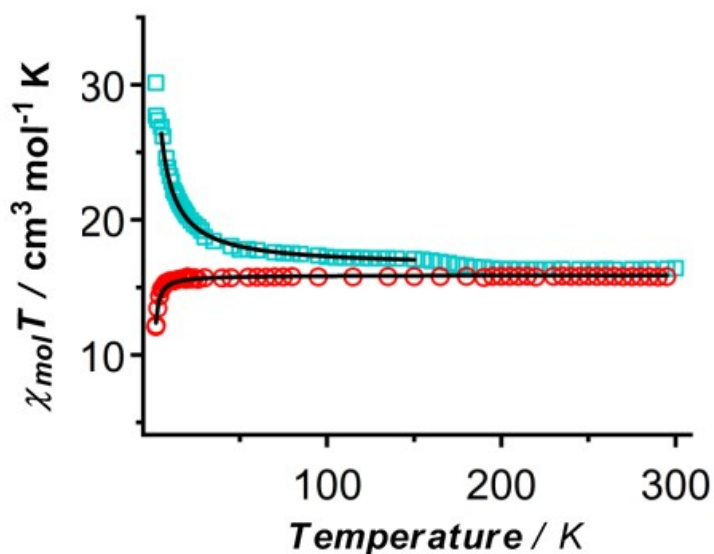


Figure S8. $\chi_{\text{mol}}T$ vs. T plots (a) before (red) and after irradiation (sky blue) of **1d** in the range of 300 K – 2 K with the theoretical curves (solid lines) according to eq. S1 and a rhombic four spin model, respectively.

S-10.

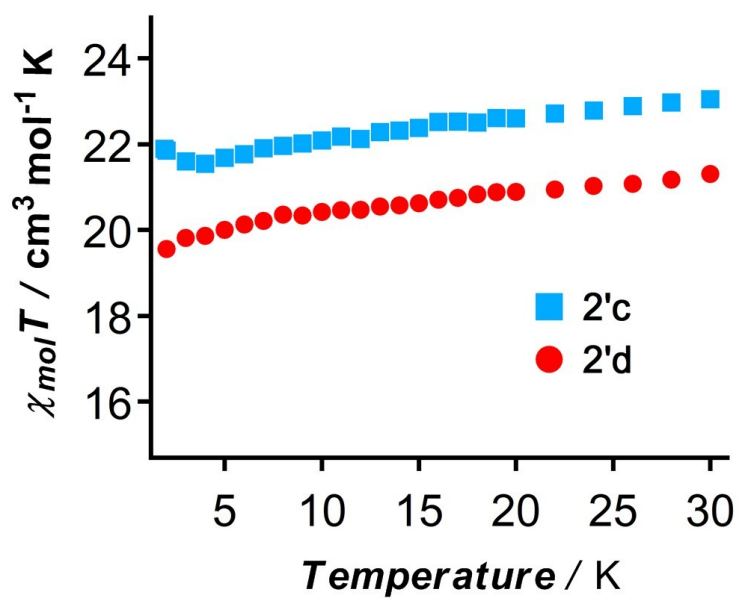


Figure S9. $\chi_{\text{mol}}T$ vs. T plots before and after irradiation of 2'd

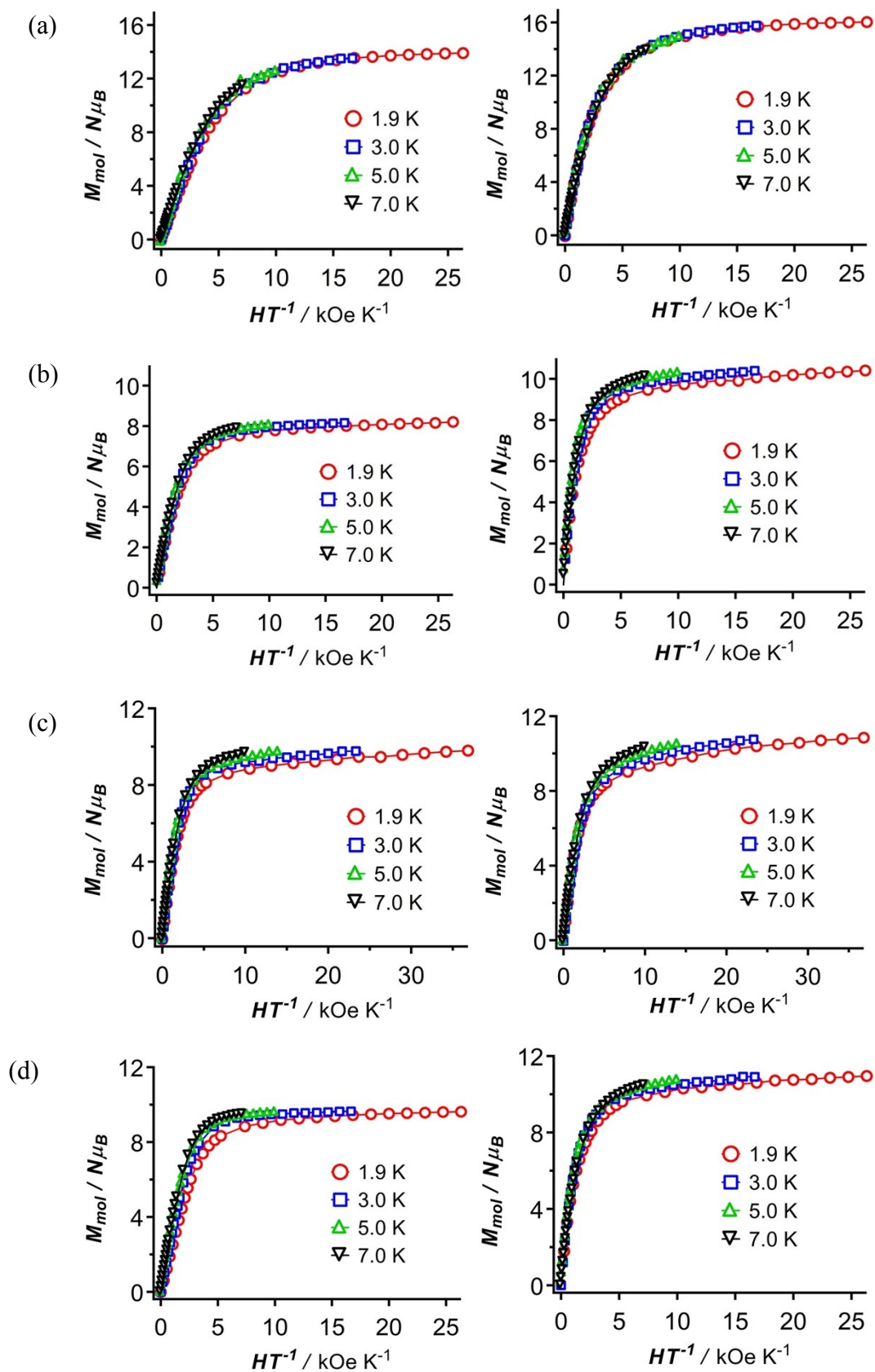


Figure S10. M_{mol} vs. H/T plots before (left) and after (right) irradiation of **1d** (a), **2d** (b), **2'd** (c), and **3d** (d).

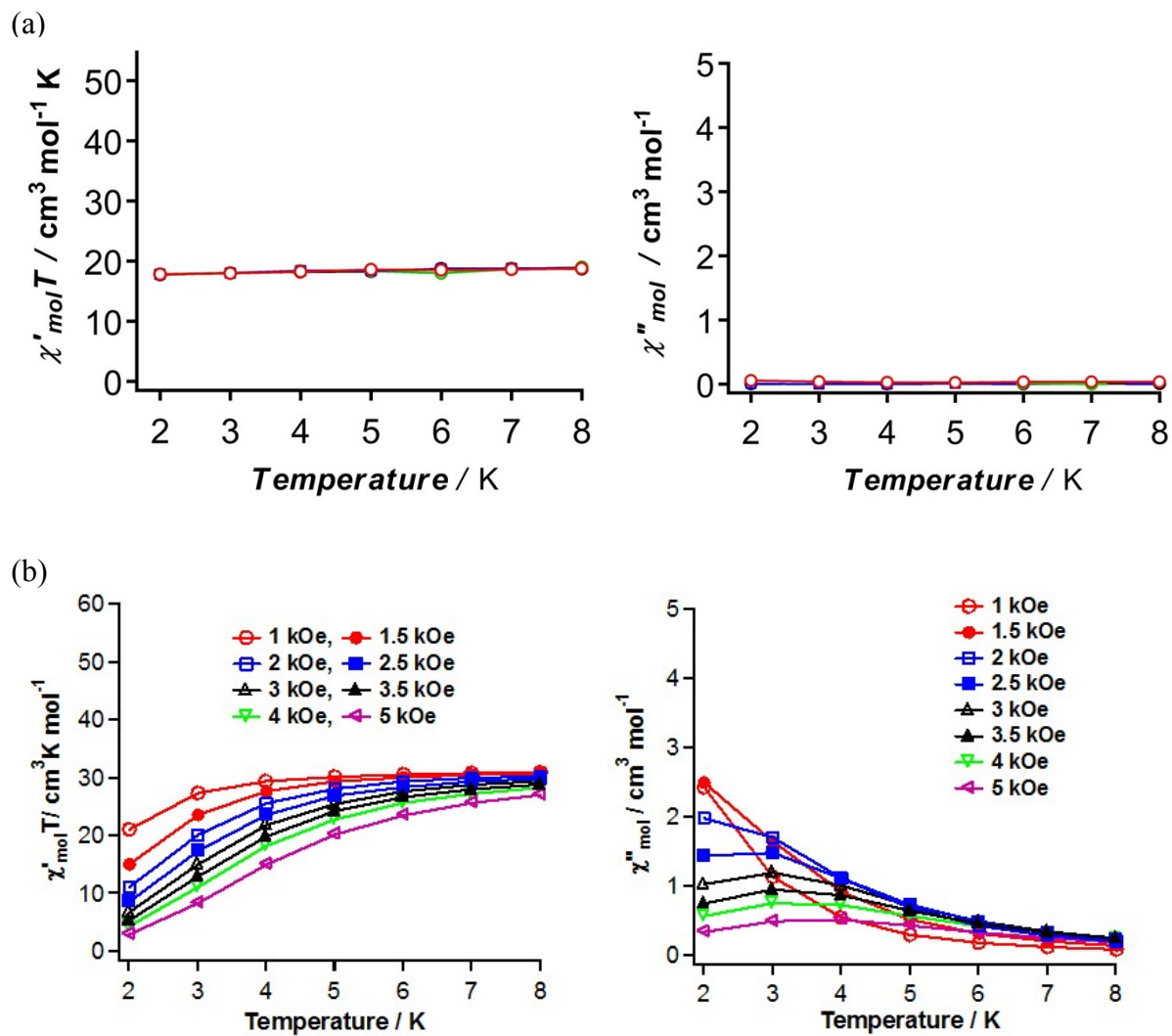


Figure S11. Plots of $\chi'_{mol}T$ vs. T (left) and χ''_{mol} vs. T (right) at 1000 Hz in the absence (a) and presence (b) of given dc field before irradiation of **2d** (3.9 Oe ac field).

S-13.

Table S3. The parameters obtained from the extended Debye model for the ac magnetic susceptibilities of **2c** at given temperatures.

T / K	$\chi_s / \text{cm}^3 \text{mol}^{-1}$	$\chi_T / \text{cm}^3 \text{mol}^{-1}$	τ / sec	α
1.8	4.7153	17.4995	1.61531	0.504361
1.9	4.78687	17.1715	0.566046	0.448258
2.1	4.39194	15.8956	0.237916	0.472878
2.2	4.17644	15.2997	0.102131	0.451552
2.3	4.08357	15.0021	0.061508	0.44081
2.4	3.64698	14.334	0.015569	0.411417
2.6	3.29364	13.7767	0.005529	0.386945
2.8	3.00268	13.2457	0.002311	0.358451
3.2	3.46688	12.27	0.000745	0.264284
3.4	3.58046	11.7888	0.000463	0.225182
3.6	3.78817	11.3659	0.000307	0.195324
3.8	2.99412	10.9476	0.000173	0.195845
4.0	4.45017	10.5091	0.000156	0.158905

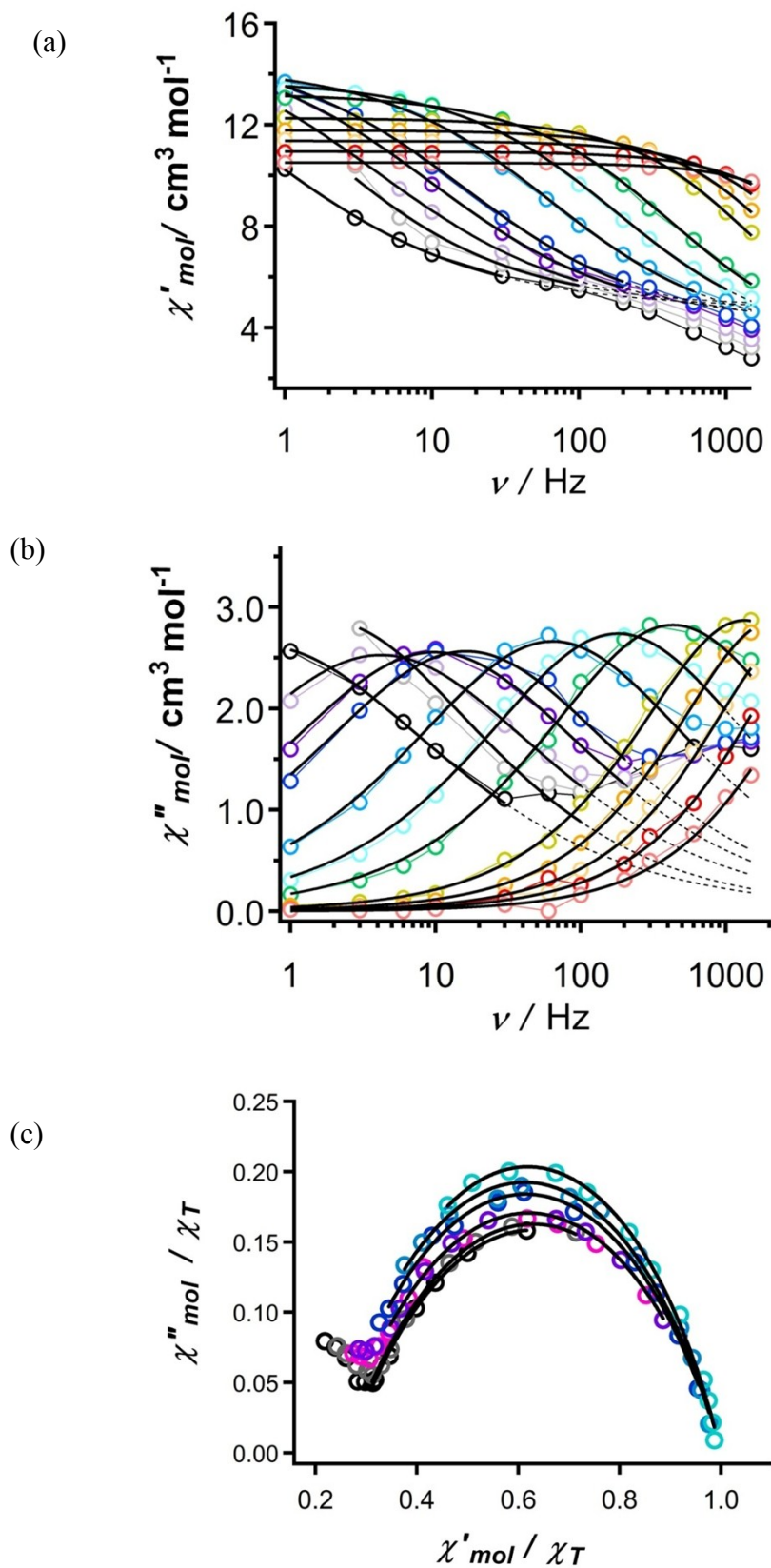


Figure S12. Plots of χ'_{mol} vs. *frequency* (a), χ''_{mol} vs. *frequency* (b) at 4.0 – 1.8 K and Cole – Cole (c) of **2c** at selected temperatures in 4.0 – 1.8 K (3.9 Oe ac field). The black solid lines and black dotted lines are the fitted lines and expected lines, respectively.

S-15.

The Cole-Cole plots for **2c** were fitted by the equation S2 for the multiple relaxation process to afford the parameters of τ_1 , τ_2 , α_1 , α_2 , and β . The obtained parameters are listed in Table S4. The values of the relaxation time, τ_1 and τ_2 , at given temperatures were plotted according to Arrhenius law. From the Arrhenius plot (Figure S13), U_{eff}/k_B of 31 and 9.1 K and τ_0 of 5.9×10^{-8} and 6.5×10^{-6} sec were obtained.

$$\chi'' = (\chi_T - \chi_S) \left\{ \frac{\beta(\omega\tau_1)^{1-\alpha_1} \cos 1/2\alpha_1\pi}{1 + 2(\omega\tau_1)^{1-\alpha_1} \sin 1/2\alpha_1\pi + (\omega\tau_1)^{2(1-\alpha_1)}} + \frac{(1-\beta)(\omega\tau_2)^{1-\alpha_2} \cos 1/2\alpha_2\pi}{1 + 2(\omega\tau_2)^{1-\alpha_2} \sin 1/2\alpha_2\pi + (\omega\tau_2)^{2(1-\alpha_2)}} \right\} \quad \text{eq. S2)}$$

Table S4. Parameters obtained from the fitting with the equation S2 for the multiple relaxation process.³⁾

	1.8 K	1.9 K	2.0 K	2.1 K	2.2 K	2.4 K	2.6K
τ_1		1.1	2.4×10^{-1}	1.2×10^{-1}	7.0×10^{-2}	2.0×10^{-2}	1.1×10^{-2}
α_1		0.44	0.40	0.40	0.39	0.36	0.27
τ_2	1.0×10^{-3}	7.1×10^{-4}	6.7×10^{-4}	5.7×10^{-4}	3.6×10^{-4}	2.8×10^{-4}	
α_2	0.32	0.26	0.180	0.160	0.16	0.12	
β^*	0.64	0.74	0.72	0.74	0.73	0.76	0.46

* β denotes the ratio of a slow magnetic relaxation component at given temperatures.

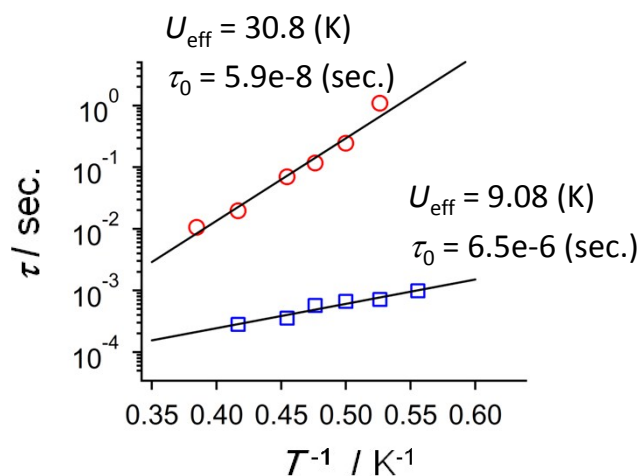


Figure S13. Arrhenius plots of two species for **2c**.

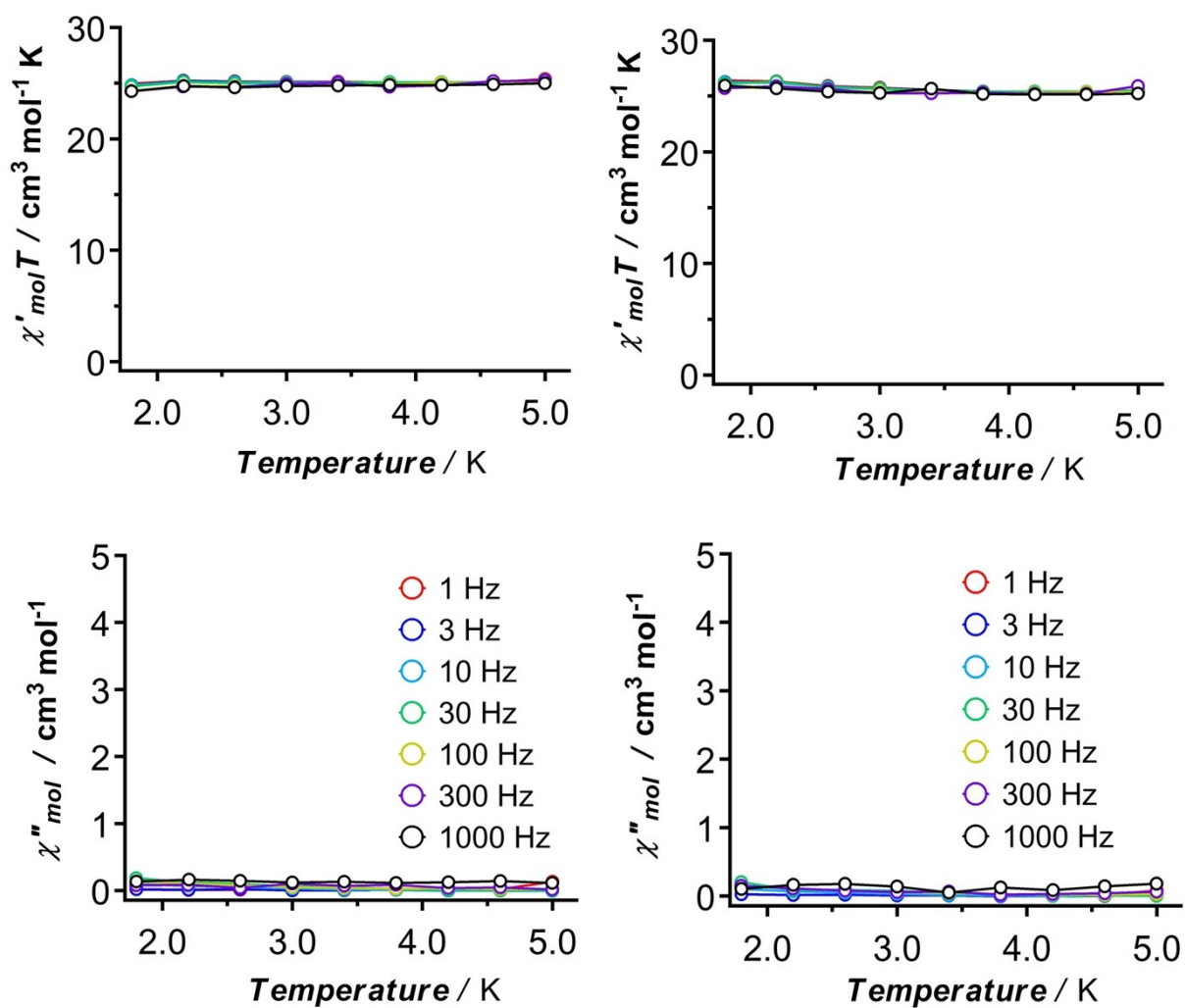


Figure S14. Plots of $\chi'_{mol}T$ vs. T (upper) and χ''_{mol} vs. T (down) at zero dc field with 3.9 Oe ac field of **2'd** (left) and **2'c** (right).

S-17.

Table S5. The parameters obtained from the extended Debye model for the ac magnetic susceptibilities of **3d** (A) and **3c** (B) at given temperatures.

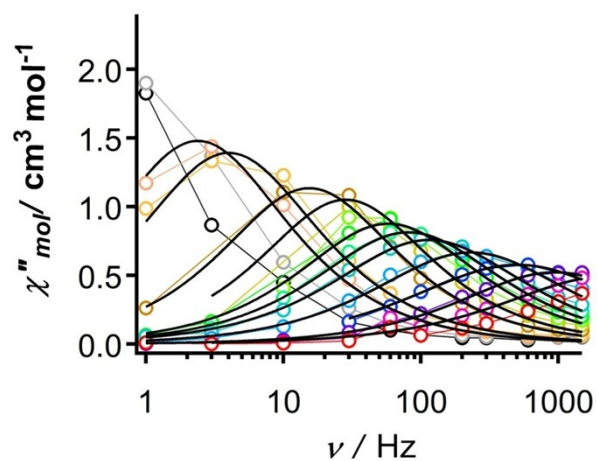
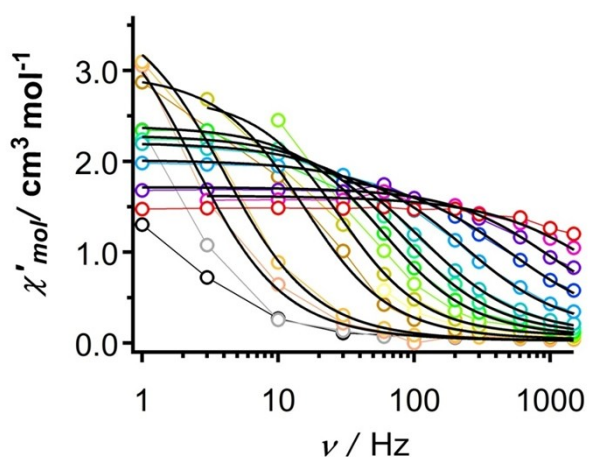
(A) **3d**

T / K	$\chi_s / \text{cm}^3 \text{mol}^{-1}$	$\chi_T / \text{cm}^3 \text{mol}^{-1}$	τ / sec	α
5.0	0.022821	3.96373	0.418405	0.180213
5.5	0.020342	3.73257	0.249668	0.180782
7.0	0.033317	2.9717	0.064867	0.162691
8.0	0.071397	2.72789	0.035245	0.147749
8.5	0.062294	2.39418	0.017219	0.179385
9.0	0.077283	2.29065	0.012302	0.192861
9.5	0.076538	2.2087	0.008757	0.213413
10	0.111403	2.01635	0.004324	0.222296
11	0.101008	1.89657	0.001987	0.272688
12	0.244813	1.7169	0.001061	0.21423
13	0.110855	1.62321	0.000444	0.265851
14	0.022821	3.96373	0.418405	0.180213

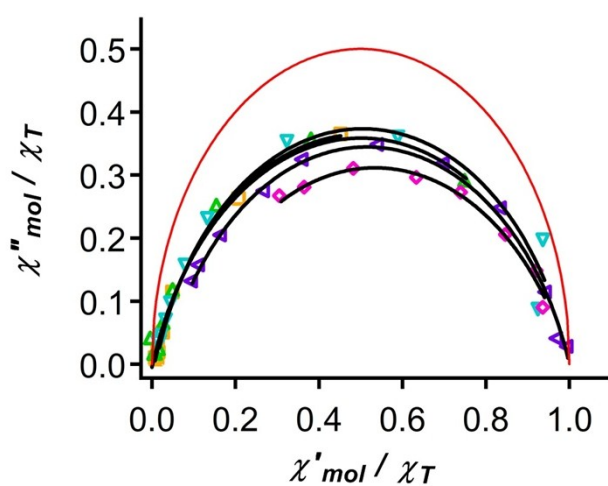
(B) **3c**

T / K	$\chi_s / \text{cm}^3 \text{mol}^{-1}$	$\chi_T / \text{cm}^3 \text{mol}^{-1}$	τ / sec	α
1.8	0.03668	23.1008	0.485611	0.395491
1.9	-0.02474	23.8821	0.346931	0.399062
2.0	0.015723	23.0617	0.218336	0.381735
2.1	-0.04795	22.5263	0.142201	0.383274
2.2	0.088056	21.2827	0.095699	0.353463
2.4	0.096759	19.3229	0.036745	0.330266
2.7	0.14887	16.7128	0.012045	0.308483
3.0	0.137317	14.755	0.004679	0.305276
3.3	-0.16243	13.2373	0.001952	0.327284
3.6	-0.63958	11.8322	0.000858	0.348503
3.9	-2.2866	10.7188	0.000314	0.397744

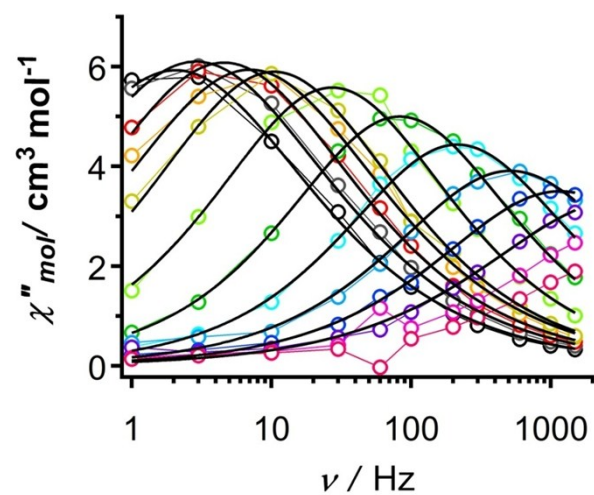
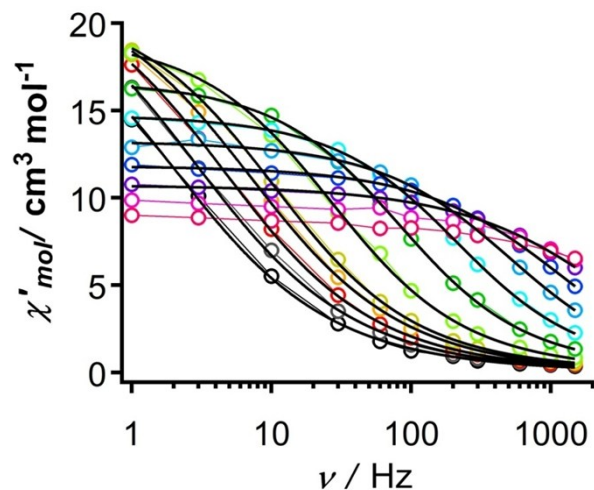
S-18. Debye plots (13 – 5 K) of **3d**



Cole-Cole plot (14 – 2.5 K) of **3d**



Debye plots (3.9 – 1.8 K) of **3c**



Cole-Cole plot (3.9 – 1.8 K) of **3c**

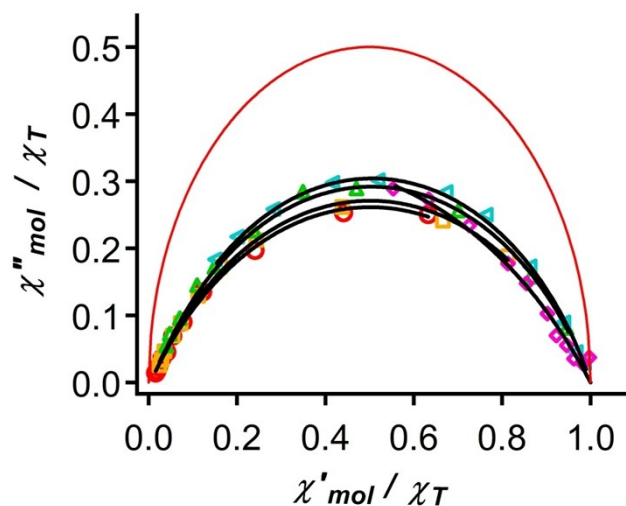


Figure S15. Plots of χ'_{mol} vs. *frequency* (upper), χ''_{mol} vs. *frequency* (middle), and Cole – Cole (bottom) at zero dc field with 3.9 Oe ac field of **3d** (left) and **3c** (right). The black and red lines are the fitted lines and the theoretical lines for $\alpha = 0$, respectively.

References.

- 1) L. Engelhardt, M. Luban *Dalton Trans.* **2010**, 39, 4687-4692.
- 2) L. Engelhardt, C. Garland, C. Rainey, A. Freeman, *arXiv.org, e-Print Archive, Condensed Matter in Cornell University Library*, **2013**, 1-6.
- 3) (a) Y.-N. Guo, G.-F. Xu, Y. Guo, J. Tang *Dalton*. **2011**, 40, 9953-9963. (b) Y.-N. Guo, G.-F. Xu, P. Gamez, L. Zhao, S.-Y. Lin, R. Deng, J. Tang, H.-J. Zhang *J. Am. Chem. Soc.* **2010**, 132, 8538-8539.